Above Room Temperature Ferromagnetism in Gd_2B_2 Monolayer with High Magnetic Anisotropy

Taylan Gorkan, Erol Vatansever, Ümit Akıncı, Gökhan Gökoglu, Ethem Aktürk,* and Salim Ciraci*

Cite This: *J. Phys. Chem. C* 2020, 124, 12816−12823

Read Online

ACCESS | Metrics & More | Article Recommendations | SI Supporting Information

ABSTRACT: The realization of 2D ultrathin crystals with a ferromagnetic ground state that is sustainable at room temperature has been a real challenge now. By combining ab initio density functional theory with Monte Carlo simulations, we predicted a new 2D structure, Gd_2B_2 monolayer, which maintains its mechanical stability at elevated temperatures. More remarkably, it has a ferromagnetic ground state with high permanent magnetic moment, which persists far above room temperature. It exhibits high magnetocrystalline anisotropy along particular directions. We find also that both its magnetic anisotropy and Curie temperature can largely be altered by applied strain providing an excellent magnetoelastic tunability. This novel 2D crystal with high magnetic moment and Curie temperature combined with high structural and thermal stability can offer critical applications in magnetoelectronics.
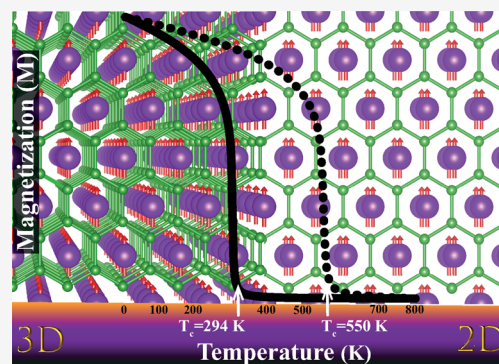
INTRODUCTION

Intense research over the past three decades has shown that the dimensionality of periodic systems ranging from 0 to 3 becomes decisive in their mechanical, electronic, and magnetic properties. Electrons in lower dimensionality have a quantization different from that in 3D. Quantized conductance observed in 1D atomic chains, integer and fractional quantum Hall effect, and massless Fermion behavior in 2D are well-known manifestations of dimensionality effects. As the debates on the mechanical stability of 2D monolayers continue, several strictly 2D crystals have been predicted and/or synthesized[1−7] in the laboratories showing diverse electronic states, such as metals, semimetals, semiconductors, half-metals, and topological insulators. Even electronic nanodevices have been fabricated from these 2D materials.

Robust intrinsic 2D magnetic materials are highly desired for various applications from spintronics to information technology and data storage. Whether a magnetic state above the room temperature can be attained in 2D structures has been now a great challenge.[8−15] Theoretical studies using 2D Ising, XY-, and Heisenberg models have indicated that the long-range magnetic order in 2D crystals can depend on the dimensionality of spins resulting in the Curie temperature, $T_c > 0$. The superexchange interaction has been considered as the prime mechanism for the ferromagnetic states. For various technological applications, 2D intrinsic ferromagnets with a high Curie temperature, T_c are desirable.[16] Nowadays, intense experimental and theoretical studies are being carried out on 2D ferromagnetic materials to develop spintronic devices operating at room temperature. MXene[15,17] and MBene[18,19] systems, as wide families of 2D magnetic structures, receive considerable attention owing to their magnetic nature and eligibility for spintronics. Recent synthesis of a member of 2D transition metal trihalides CrI_3[20] and transition metal chalcogenides (TMC) $Cr_2Ge_2Te_6$[21] showing a ferromagnetic order have brought the second and third neighbor exchange interaction in 2D magnetic crystals together with their magnetic anisotropy into focus. 2D intrinsic magnetism was found in CrI_3 bilayer which behaves as a layered antiferromagnet with an electrically controlled metamagnetic transition between antiferromagnetic and ferromagnetic phases.[22] The suppression of the long-range magnetic order in 2D materials can be counteracted by magnetic anisotropy. Pristine $Cr_2Ge_2Te_6$ atomic layers are two-dimensional van der Waals ferromagnet with a transition temperature which can easily be controlled by very small fields around ∼0.3 T.[21] $MnBi_2Te_4$ family van der Waals layered materials have been shown to exhibit 2D ferromagnetism with an out-of-plane easy axis in a single layer with various exotic physical effects like quantum anomalous Hall effect.[23] It was demonstrated that Fe_3GeTe_2 in the monolayer form exhibits robust 2D ferromagnetism with strong perpendicular (out-of-plane) anisotropy and low Curie temperature ∼130 K.[24,25] In Fe_3GeTe_2, partially filled Fe-d orbitals around the Fermi level result in itinerant ferromagnetism of the bulk structure
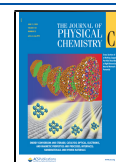
which shows strong magnetocrystalline anisotropy.[26] It is expected that the anisotropy stabilizes the long-range ferromagnetic order in Fe_3GeTe_2 monolayers. Other members of transition metal halides family, i.e., RuX_3 (X = Cl, Br, and I),[27,28] have been investigated using density functional theory (DFT) and Monte Carlo simulations (MC) yielding relatively low Curie temperatures, ∼14 K for RuCl, 13 K for RuBr, and ∼2 K for RuI. $MnSe_2$[29] monolayer system has been found also to exhibit ferromagnetic order at room temperature.

As for the 2D nonmagnetic materials, they can acquire a ferromagnetic behavior via a structural defect,[30] adsorbed atoms,[31] and applied strain.[32−34] Also, the nonmagnetic nature of the most common and well-known 2D materials may render applications in magnetoelectronics and spintronics through the incorporation of a ferromagnetic material into a device.[35]

Among the heavy rare earth metals, the most attractive one is gadolinium (Gd)[36−38] which has half-filled and well-localized 4f subshell leading to ferromagnetic behavior with high saturation magnetization.[39] However, as experimentally certified, the ferromagnetic order of Gd single crystals is destroyed when the temperature exceeds 293 K.[40] Bulk Gd is a ferromagnetic metal with a magnetic moment per Gd atom of 7.55 μ_B.[40] 3D GdB_2 crystal is a member of the hexagonal rare earth metal diborides family with AlB_2-type structure conforming to $P6/mmm$ space group symmetry.[41] In Figure 1a, the optimized structure of bulk GdB_2 is given with
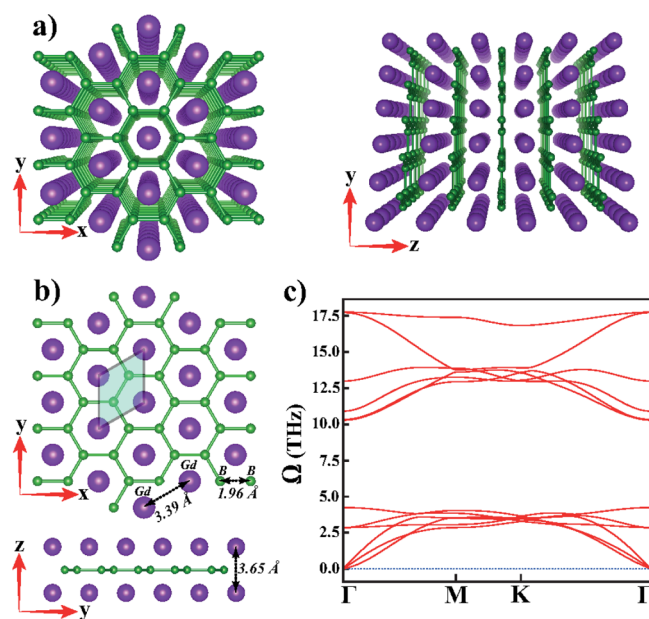
Figure 1. (a) Top and side perspective views of 3D bulk GdB_2 crystal with AlB_2-type hexagonal lattice. (b) Top and side views of Gd_2B_2 monolayer with hexagonal lattice showing the optimized primitive unit cell and other structural parameters. Purple and green balls represent Gd and B atoms, respectively. (c) Phonon frequencies, Ω versus **k** of Gd_2B_2 monolayer calculated from the first-principles along the high-symmetry directions of Brillouin zone.

alternating hexagonal B and Gd planar layers, whereby Gd atoms are located above the centers of the hexagons of B atoms at a distance of 1.89 Å (experimental value[41] being ∼1.97 Å). This way Gd atoms are ordered to form centered hexagons of hexagonal closed packed (hcp) [0001] surface.

In this study we predict a new 2D monolayer derived from bulk gadolinium diboride, namely free-standing Gd_2B_2

monolayer, which is stable and has a robust planar geometry. This structure is simply a borophene monolayer capped by Gd atoms from both side. Gd atoms, by themselves, stabilize borophone by donating electrons to fill its empty π-bands to transform it to a stable graphene like, planar honeycomb structure. Even more remarkable is that Gd_2B_2 monolayer is a ferromagnetic metal; its ferromagnetic state can sustain above the room temperature as high as $T_c = 550$ K with a high magnetic moment of $\mu = 7.30$ μ_B per Gd atom. Additionally, high magnetic anisotropy and high critical temperature of this 2D crystal can be tuned by applied strain. This new monolayer heralds also a new family of 2D structures, M_2X_2 (M being heavy rare earth or transition metal atoms and X being group-III or group-V elements) with unusual magnetic properties. These predictions are obtained from our study based on the first-principles, spin-polarized Density Functional Theory including Hubbard U correction for on-site Coulomb interaction, which are combined with Monte Carlo simulations. The details of our calculations are presented in the Supporting Information.

The structure of Gd_2B_2 monolayer described in Figure 1b consists of a planar honeycomb structure of B atoms or borophene[42,43] having the planes of Gd atoms at either side forming a Gd bilayer in AA stacking pattern. Here Gd atoms are adsorbed above the hollow sites of the honeycomb structure of borophene. The distance between B and Gd layers is 1.83 Å. The average cohesive energy of the fully relaxed Gd_2B_2 monolayer calculated to be 6.18 eV is rather high and is only 770 meV smaller than that of bulk GdB_2 indicating an energetically favorable structure. Despite this high cohesive energy, we also performed an extensive analysis of stability to ensure that Gd_2B_2 monolayer is a dynamically and thermally stable structure. The absence of any imaginary frequencies calculated for optimized structures of Gd_2B_2 monolayer, especially for $\mathbf{k} \rightarrow 0$ and of any vibrational anomalies in phonon dispersion presented in Figure 1c verify the dynamical stability. We also perform constant temperature equilibrium molecular dynamic (MD) simulations to verify whether Gd_2B_2 monolayer can sustain high temperature thermal excitations. The structure is kept at 300, 600, and 1000 K temperatures for 2 ps. It is observed that the structure is well-preserved without any significant deformation even at 1000 K.

The electronic band structure and density of states (DOS) of the optimized, free-standing Gd_2B_2 monolayer display a metallic character as seen in Figure 2a. Part of the bands below −2 eV with broken spin-degeneracy mimics the σ-bands derived from B-sp^2 orbitals. The π-bands derived from π-orbitals of B atoms slightly hybridized with Gd orbitals are located above −2 eV and set the Fermi level. Other bands below the Fermi level are derived from the Gd-5d and Gd-6s orbitals. According to the Bader analysis, each Gd atom donate ∼0.8 electrons to borophene. This way the empty π-bands of borophene becomes occupied and hence π-bonds maintaining the planar geometry are constructed. At the end, the planar borophene honeycomb structure is stabilized by Gd bilayer above and below to transform to a robust, graphene-like electronic structure. Flat bands ∼4 eV above the Fermi level are derived from Gd-4f orbitals. Spin-split bands and the total and atom projected densities of spin-up and spin-down states clearly show the magnetic ground state of Gd_2B_2. Energy bands including the spin−orbit coupling (SOC) are in conformity with above findings. The isosurfaces of the difference charge density, $\Delta\rho$, and the spin density $\Delta\rho_S = \rho_T \downarrow - \rho_T \uparrow$ in Figure
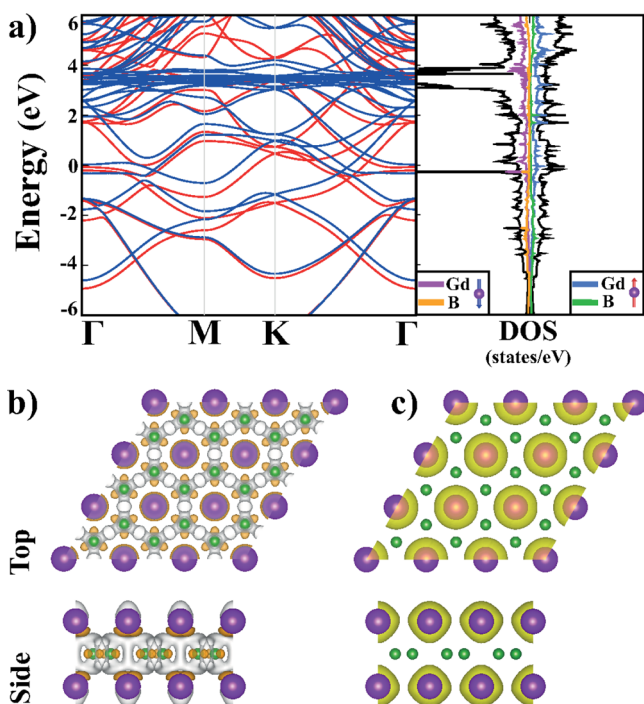
Figure 2. Spin polarized electronic energy band structures and corresponding total and atom projected densities of states of spin-up and spin-down states. The zero of energy is set at the Fermi level. (b) Isosurfaces of the difference charge density, $\Delta\rho$. White and gold regions indicate charge accumulation and charge depletion upon the formation of monolayer relative to its free constituent atoms. (c) Spin density ρ_S located around Gd atoms displays a ferromagnetic order.

2b,c unveil valuable details concerning the bonding in compliance with the above discussion and the magnetic ground state. The σ-bonds constructed from the bonding combination of nearest B-sp^2 orbitals with a bond charge at the middle of B−B bonds and the π-bonds derived from mostly B-p$_z$ orbitals but filled by the electrons donated by Gd atoms. The spin density isosurfaces in Figure 2c indicates a net spin-density and hence magnetic moment at Gd atoms; but no net spin density at B atoms. Accordingly, one can view the Gd$_2$B$_2$ monolayer as a nonmagnetic borophene layer caped by magnetic Gd layers.

The magnetic ground state of Gd$_2$B$_2$ monolayer is determined by calculating the total energies of ferromagnetic (FM) and antiferromagnetic (AFM) states. The total energies are calculated with Generalized Gradient Approximation, GGA including Hubbard U correction for on-site Coulomb interaction,[44] since the realistic description of the electron−electron interaction is essential for the determination of the correct magnetic ground state. In a previous study, it was shown that DFT+U scheme largely affects the magnetic ground state of bulk GdB$_2$ with only small deviations in lattice constants.[45] The unit cell (or supercell), which is used in the calculations is described in Figure 3, where FM and three different AFM spin configurations are illustrated. We found that FM state is most favorable energetically among various spin configurations with the energy differences ∼0.12, ∼0.26, and ∼0.28 eV between FM and AFM-1, AFM-2, and AFM-3 configurations in Figure 3, respectively. Accordingly, free-standing Gd$_2$B$_2$ monolayer has ∼31.23 μ_B total magnetic moment per rectangular unitcell with contributions of ∼7.30 μ_B magnetic moment of each Gd atom. This value is slightly
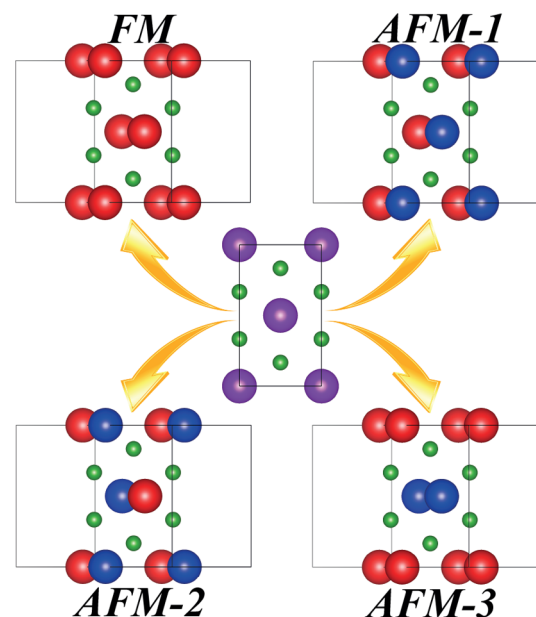
Figure 3. Rectangular unitcell (or supercell) containing three nearest neighbors of Gd atoms with one ferromagnetic, FM and three different antiferromagnetic, AFM-1, AFM-2, and AFM-3 spin configurations. The structures are rotated around y-axes by 15° to clarify atomic positions in the cell. Red and blue balls indicate Gd atoms with up and down magnetic moments, respectively. Boron atoms are indicated by small-green balls.

larger than magnetic moment of Gd atom in 3D crystal which is 7.17 μ_B.

Magnetocrystalline anisotropy energy, E_{MA} is an important quantity to reveal the effect of magnetic field on the material. The large E_{MA} is also a desired property for spintronic applications.[46] Taking the[001] direction as the easy axes of magnetization, we calculate E_{MA} values along the [100], [010], [110], and [111] hard axes according to the expression, $E_{MA} = (E_{[hkl]} - E_{[001]})/4$. Here $E_{[hkl]}$ and $E_{[001]}$ are the total energies with magnetization in related directions. Due to the importance of strain effect[13,47] on magnetocrystalline aniso-tropy, we also investigated the variation of E_{MA} under uniform, biaxial compressive and tensile strains as given in Table 1. E_{MA} values are rather large indicating high magnetic anisotropy, they also display dramatic changes with applied strain. As an example, while the [100]-direction is the hardest axes of magnetization, it becomes an easy axis of magnetization under

Table 1. Magnetocrystalline Anisotropy Energies E_{MA} (μeV per Gd Atom) and the Curie Temperatures T_c (K) Predicted for Gd$_2$B$_2$ Monolayer under Compressive (−) and Tensile (+) Strain ϵ

ϵ (%)	$E_{[100]-[001]}$	$E_{[010]-[001]}$	$E_{[110]-[001]}$	$E_{[111]-[001]}$	T_c
−8	34	323	163	30	395
−6	92	155	104	−10	365
−4	993	665	802	571	480
−2	1210	970	1151	706	480
0	1706	1167	1495	915	550
2	1562	1819	1684	1127	570
4	755	1246	1051	653	480
6	1269	1342	1356	913	480
8	1327	1048	1191	766	275
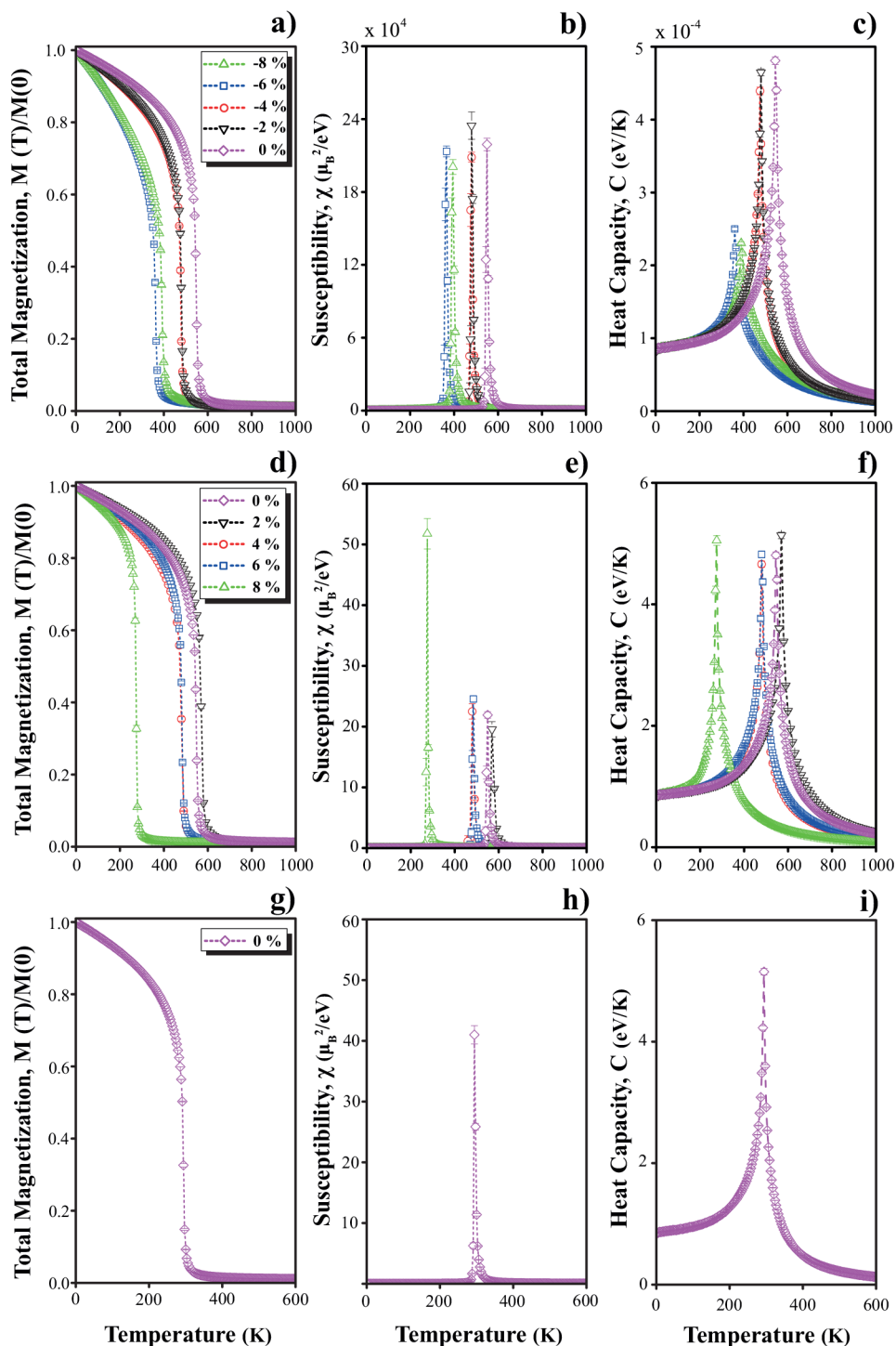
Figure 4. Normalized magnetization, $M(T)/M(0)$; magnetic susceptibility, χ; heat capacity C as a function of temperature calculated for Gd_2B_2 monolayer under compressive strain $\epsilon < 0$ and tensile strain, $\epsilon > 0$. Panels a–c are values calculated for $0 \geq \epsilon \geq -8\%$. Panels d–f are for $8\% \geq \epsilon \geq 0$. Panels g–i correspond to the curves obtained for bulk GdB_2 for $\epsilon = 0$ case.

$\epsilon = -8\%$ compressive strain. In particular, a tensile strain as small as 2% induces a remarkable change so that [010]-direction becomes a hard axes of magnetization.

Under thermal excitations, the ordered ferromagnetic phase discussed above changes to the disordered paramagnetic state at a critical temperature or Curie temperature, T_c. The critical temperature, which determines the potential of a ferromagnetic crystal in various technological applications is of prime importance. As for atomically thin 2D crystals, the value of

T_c becomes even more critical. In what follows, we will consider Gd_2B_2 monolayer under selected compressive and tensile strain. Using spin–spin interactions energies between first, second and third nearest neighbor spin pairs obtained from DFT (see Table S1 in the Supporting Information) in Monte Carlo simulations we calculate the variation of the total magnetization $M(T)$, magnetic susceptibility $\chi(T)$, and heat capacity $C(T)$ as a function of temperature. Then we determine the Curie temperature of Gd_2B_2 monolayer

corresponding to unstrained and strained states. The details of Monte Carlo simulations are presented in the Supporting Information.

The value of the Curie temperature, T_c, of the unstrained Gd_2B_2 monolayer is predicted to be T_c = 550 K, but it decreases under both tensile and compressive strains, except for 8% tensile strain. High Curie temperature predicted for Gd_2B_2 monolayer is an important feature of this material for spintronic applications. The results obtained from the Monte Carlo simulations are summarized in Figure 4. The variations of total magnetization $M(T)$, magnetic susceptibility $\chi(T)$, and specific heat $C(T)$ with temperature, T, calculated for selected biaxial compressive strain, $0 \geq \epsilon \geq -8\%$, are presented in Figure 4a−c. Those calculated for varying applied biaxial strain, $8\% \geq \epsilon \geq 0$ are given in Figure 4d−f. It is noted that all magnetization curves depicted here are normalized to its ground state value at $T = 0$ K. As shown in Figure 4a, as the temperature raises starting from relatively lower temperatures, the total magnetization decreases from its saturation value due to the increasing thermal fluctuations. The strongly ferromagnetic character observed in Gd_2B_2 monolayer structure disappears when the temperature increases further and reaches the Curie temperature T_c, where Gd_2B_2 monolayer undergoes a phase transition from ferromagnetic to paramagnetic phases. Our Monte Carlo simulation results indicate that the physical mechanism briefly described here sensitively depends on the applied strain. Hence, T_c tends to decrease with increasing biaxial compressive and tensile strain starting from unstrained, $\epsilon = 0$, case corresponding to T_c = 550 K. As seen in Figure 4b,c, $\chi(T)$ and $C(T)$ curves diverge at $T = T_c$ indicating a second-order phase transition. The phase transition temperatures, 480, 480, 365, and 395 K corresponding to the applied compressive strain values of −2%, −4%, −6%, and −8%, respectively, are inferred from the peak positions of $\chi(T)$ and $C(T)$ curves calculated for the selected strain values. The similar analysis is done also for Gd_2B_2 monolayer under the tensile strain, as depicted in Figure 4d−f showing strong dependence on the applied tensile strain. Notably, all transition temperatures are above the room temperature, except for ϵ = 8% case with T_c = 275 K. Numerical values calculated for T_c are also presented in Table 1. These results suggest that the Gd_2B_2 monolayer may find critical applications in magneto-electronics with high magnetic moments and high Curie temperature, which are tunable with the biaxial compressive and tensile strain.

For the sake of completeness, we also present $M(T)/M(0)$, $\chi(T)$, and $C(T)$ curves calculated for GdB_2 in bulk phase for ϵ = 0 case, as demonstrated in Figure 4g−i. Based on DFT calculations, spin−spin couplings J_1, J_2, and J_3 are estimated to be 1.477, 1.136, and 0.872 in units of meV, respectively. Similarly, we have calculated magnetic anisotropy energies as $E[100] - E[001]$, $E[010] - E[001]$, $E[110] - E[001]$, and $E[111] - E[001]$, 2840, 2810, 2830, and 1990 in units of μeV, respectively. It is worth noting that we followed the same simulation protocol defined for the Gd_2B_2 monolayer, except for the temperature range. Our MC simulations suggest that bulk GdB_2 shows a ferromagnetic character below the Curie temperature, supporting the predictions done by DFT calculations. According to the thermal variations of the magnetic susceptibility and specific heat curves, the Curie temperature is estimated as 294 K, which is very close to the room temperature. It should be noted that the recent experimental findings of Gencer et al.[48] pertain to GdB_2 in

bulk phase in agreement with our findings, and hence they validate our method used in the present study. When the temperature approaches this value, both magnetic susceptibility and specific heat curves tend to diverge, indicating a second order phase transition as in the case of 2D Gd_2B_2 monolayer for all considered strain values. This result suggests that critical behavior of the magnetic materials can depend on the geometry/dimensionality: As already mentioned, the critical temperature is 550 K for the Gd_2B_2 monolayer, whereas it is 294 K for the bulk phase for the ϵ = 0 case.

We also note that spin waves may play an important role in 2D magnets. Spin wave theory has been successfully applied for 2D[49] and quasi 2D[50] systems in order to capture the low-temperature properties of the magnetic systems with anisotropy, which is weak compared to the exchange interaction. Critical temperature values predicted in this work may be verified by the renormalized spin-wave theory.

DISCUSSION AND CONCLUSIONS

Present analysis of the Gd_2B_2 monolayer indicates that Gd atoms located above and below the centers of borophene hexagons maintain the planar stability by donating electrons to the perpendicular π-bonds of B atoms. This way, the π-bands derived mainly from B-p_z orbitals become occupied. The metallicity of Gd_2B_2 monolayer is acquired through π-bands of B as well as $5d - 6s$ orbitals of Gd, which slightly hybridizes with the former. However, the ferromagnetic state of the monolayer is completely indigenous to the spin polarized states of Gd layers. Even though the Gd_2B_2 monolayer is derived from the 3D GdB_2 crystal in the foregoing discussion, it can also be synthesized from the bare borophene monolayer. Much recently, it has been demonstrated that a single borophene layer can be synthesized on the Al(111) surface.[43] Theoretical studies demonstrated how the stability of the hexagonal borophene monolayer is maintained by the adsorption of metal atoms above the centers of boron hexagons.[42,51−53] As pointed out in those studies, centers of hexagons constitute preferred adsorption sites for free metal M atoms to form a MB_2 monolayer. Interestingly, our analysis performed by using ab initio phonon calculations has indicated that a free-standing GdB_2 monolayer is also dynamically stable and has a ferromagnetic ground state. The latter being another new magnetic 2D monolayer can also serve as a precursor structure for the growth of the Gd_2B_2 monolayer: By transferring GdB_2 to another inert surface and by covering its other surface also by Gd atoms the growth of Gd_2B_2 can be realized. Calculated chemisorption energy of 3.1 eV per Gd atom assures strong interaction between Gd and borophene and present evidence for the feasibility of growth. Actually, not only a borophene honeycomb structure but also other stable phases of borophone can serve as a substrate to grow magnetic monolayers covered by heavy rare-earth or transition metal atoms. Additionally, one can consider that similar free-standing or supported magnetic monolayers of M_2X_2 type (M being either heavy rare-earth or transition metal atoms and X being B, C, Si, Ge, P, As, Sb, and Bi) can be realized to exploit novel electronic and magnetic properties. Earlier, the planar or buckled monolayers of Si, Ge, P, As, Sb, and Bi were shown to be stable.[3,54,55] Recently, by the chemisorption of heavy rare-earth metal atoms above planar honeycomb structure of graphene and the buckled honeycomb structure of silicene and germanene[3] have been realized experimentally to synthesize magnetic monolayers and multilayers,[56−58] $GdSi_2$, $GdGe_2$,

EuSi$_2$, EuGe$_2$, and EuC$_6$ like GdB$_2$ monolayer predicted here. Some of these structures exhibited interesting ferromagnetic-antiferromagnetic transition with the number of layers. In the present study, we carried out structure optimization and phonon calculations from the first-principles and demonstrated that free-standing Gd$_2$Si$_2$ monolayer is stable. The calculated chemisorption energy of 2.65 eV per Gd atom shows a strong interaction between Gd and buckled silicene, even if the buckling of silicene is decreased. We think that this strong chemical interaction becomes the driving force for the growth. Briefly, these new experimental results together with our theoretical analysis present strong evidence that the synthesis of GdB$_2$ and Gd$_2$B$_2$ is affordable.

Recently, Zunger has drawn a large perspective on the design and functionality of new materials by discussing stability and synthesizability.[59] Globally thermodynamically metasable structures can also be grown by modern crystal growth techniques like molecular beam epitaxy. These structures can be forced by means of the experimental set up which restricts the chemical kinetics of constituent atoms by imposing necessary physical conditions to realize a thermodynamically unstable structure. Moreover, once a structure was constructed artificially, it can continue to exist at ambient conditions due to large energy barriers preventing it from transition to a more stable state.

Finally, we emphasize three features of Gd$_2$B$_2$ monolayer by way of conclusion: (i) It is a 2D crystal, which remains stable even at elevated temperatures. (ii) It has ferromagnetic ground state with high magnetic moment of 7.3 μ_B per Gd atom, which can sustain above room temperature; the transition from ordered magnetic state to a disordered state can take place at the critical temperature as high as 550 K. (iii) High magnetic anisotropy and high Curie temperature of Gd$_2$B$_2$ can be tuned externally by applied strain. Given these features, Gd$_2$B$_2$ monolayer and its similar allotropes, Gd$_x$B$_2$ and also their lateral and vertical heterostructures may allow the designing of diverse magnetoelectronic devices capable of operating above room temperature. The class of 2D materials represented by GdB$_2$ and Gd$_2$B$_2$ and obtained from the chemisorption of heavy rare-earth metals atoms chemisorbed to the honeycomb structures, such as brophene, graphene, silicene, germanene, blue phosphorene, hexagonal arsenene, antimonene, and bismuthene, in different coverage and decoration heralds that the quest to diverse magnetic properties in technology can be achieved in 2D materials.

■ ASSOCIATED CONTENT

ⓈI Supporting Information

The Supporting Information is available free of charge at https://pubs.acs.org/doi/10.1021/acs.jpcc.0c03304.

Additional computational methods (PDF)

■ AUTHOR INFORMATION

Corresponding Authors

Ethem Aktürk − *Department of Physics and Nanotechnology Application and Research Center, Adnan Menderes University, Aydın 09100, Turkey;* ⓞ orcid.org/0000-0002-1615-7841; Phone: +902562130835-1894; Email: ethem.akturk@adu.edu.tr; Fax: +902562135379

Salim Ciraci − *Department of Physics, Bilkent University, Ankara 06800, Turkey;* Phone: +903122901216; Email: ciraci@fen.bilkent.edu.tr; Fax: +903122664579

Authors

Taylan Gorkan − *Department of Physics, Adnan Menderes University, Aydın 09100, Turkey*

Erol Vatansever − *Faculty of Science, Physics Department, Dokuz Eylül University, İzmir 35390, Turkey*

Ümit Akıncı − *Faculty of Science, Physics Department, Dokuz Eylül University, İzmir 35390, Turkey*

Gökhan Gökoglu − *Department of Mechatronics Engineering, Faculty of Engineering, Karabuk University, Karabuk 78050, Turkey;* ⓞ orcid.org/0000-0002-2456-6397

Complete contact information is available at:
https://pubs.acs.org/10.1021/acs.jpcc.0c03304

Notes

The authors declare no competing financial interest.

■ ACKNOWLEDGMENTS

■ REFERENCES

(1) Novoselov, K. S.; Geim, A. K.; Morozov, S. V.; Jiang, D.; Zhang, Y.; Dubonos, S. V.; Grigorieva, I. V.; Firsov, A. A. Electric field effect in atomically thin carbon films. *Science* **2004**, *306*, 666−669.

(2) Novoselov, K. S.; Jiang, D.; Schedin, F.; Booth, T.; Khotkevich, V.; Morozov, S.; Geim, A. K. Two-dimensional atomic crystals. *Proc. Natl. Acad. Sci. U. S. A.* **2005**, *102*, 10451−10453.

(3) Cahangirov, S.; Topsakal, M.; Aktürk, E.; Şahin, H.; Ciraci, S. Two-and one-dimensional honeycomb structures of silicon and germanium. *Phys. Rev. Lett.* **2009**, *102*, 236804.

(4) Ataca, C.; Sahin, H.; Ciraci, S. Stable, Single-Layer MX2 Transition-Metal Oxides and Dichalcogenides in a Honeycomb-Like Structure. *J. Phys. Chem. C* **2012**, *116*, 8983−8999.

(5) Aktürk, O. U.; Özçelik, V. O.; Ciraci, S. Single-layer crystalline phases of antimony: Antimonenes. *Phys. Rev. B: Condens. Matter Mater. Phys.* **2015**, *91*, 235446.

(6) Ersan, F.; Aktürk, E.; Ciraci, S. Stable single-layer structure of group-V elements. *Phys. Rev. B: Condens. Matter Mater. Phys.* **2016**, *94*, 245417.

(7) Liu, H.; Neal, A. T.; Zhu, Z.; Luo, Z.; Xu, X.; Tománek, D.; Ye, P. D. Phosphorene: an unexplored 2D semiconductor with a high hole mobility. *ACS Nano* **2014**, *8*, 4033−4041.

(8) Jiang, Z.; Wang, P.; Xing, J.; Jiang, X.; Zhao, J. Screening and Design of Novel 2D Ferromagnetic Materials with High Curie Temperature above Room Temperature. *ACS Appl. Mater. Interfaces* **2018**, *10*, 39032−39039.

(9) Zhang, Y.; Pang, J.; Zhang, M.; Gu, X.; Huang, L. Two-Dimensional Co2S2 monolayer with robust ferromagnetism. *Sci. Rep.* **2017**, *7*, 15993.

(10) Sun, Y.; Zhuo, Z.; Wu, X.; Yang, J. Room-temperature ferromagnetism in two-dimensional Fe2Si nanosheet with enhanced spin-polarization ratio. *Nano Lett.* **2017**, *17*, 2771−2777.

(11) Wang, B.; Zhang, Y.; Ma, L.; Wu, Q.; Guo, Y.; Zhang, X.; Wang, J. MnX (X= P, As) monolayers: a new type of two-dimensional intrinsic room temperature ferromagnetic half-metallic material with large magnetic anisotropy. *Nanoscale* **2019**, *11*, 4204−4209.

(12) Jiang, Z.; Wang, P.; Jiang, X.; Zhao, J. MBene (MnB): a new type of 2D metallic ferromagnet with high Curie temperature. *Nanoscale Horiz.* **2018**, *3*, 335−341.

(13) Zheng, S.; Huang, C.; Yu, T.; Xu, M.; Zhang, S.; Xu, H.; Liu, Y.; Kan, E.; Wang, Y.; Yang, G. High-Temperature Ferromagnetism in an

Fe3P Monolayer with a Large Magnetic Anisotropy. *J. Phys. Chem. Lett.* **2019**, *10*, 2733−2738.

(14) Hu, L.; Wu, X.; Yang, J. Mn 2 C monolayer: a 2D antiferromagnetic metal with high Néel temperature and large spin−orbit coupling. *Nanoscale* **2016**, *8*, 12939−12945.

(15) Khazaei, M.; Arai, M.; Sasaki, T.; Chung, C.-Y.; Venkataramanan, N. S.; Estili, M.; Sakka, Y.; Kawazoe, Y. Novel electronic and magnetic properties of two-dimensional transition metal carbides and nitrides. *Adv. Funct. Mater.* **2013**, *23*, 2185−2192.

(16) Gibertini, M.; Koperski, M.; Morpurgo, A. F.; Novoselov, K. S. Magnetic 2D materials and heterostructures. *Nat. Nanotechnol.* **2019**, *14*, 408−419.

(17) Naguib, M.; Kurtoglu, M.; Presser, V.; Lu, J.; Niu, J.; Heon, M.; Hultman, L.; Gogotsi, Y.; Barsoum, M. W. Two-dimensional nanocrystals produced by exfoliation of Ti3AlC2. *Adv. Mater.* **2011**, *23*, 4248−4253.

(18) Zhang, H.; Xiang, H.; Dai, F.-z.; Zhang, Z.; Zhou, Y. First demonstration of possible two-dimensional MBene CrB derived from MAB phase Cr2AlB2. *J. Mater. Sci. Technol.* **2018**, *34*, 2022−2026.

(19) Ozdemir, I; Kadioglu, Y; Uzengi Akturk, O; Yuksel, Y; Akıncı, U; Akturk, E A new single-layer structure of MBene family: Ti2B. *J. Phys.: Condens. Matter* **2019**, *31*, 505401.

(20) Huang, B.; Clark, G.; Navarro-Moratalla, E.; Klein, D. R.; Cheng, R.; Seyler, K. L.; Zhong, D.; Schmidgall, E.; McGuire, M. A.; Cobden, D. H.; et al. Layer-dependent ferromagnetism in a van der Waals crystal down to the monolayer limit. *Nature* **2017**, *546*, 270.

(21) Gong, C.; Li, L.; Li, Z.; Ji, H.; Stern, A.; Xia, Y.; Cao, T.; Bao, W.; Wang, C.; Wang, Y.; Qiu, Z.; Cava, R.; Louie, S.; Xia, J.; Zhang, X. Discovery of intrinsic ferromagnetism in two-dimensional van der Waals crystals. *Nature* **2017**, *546*, 265−269.

(22) Huang, B.; Clark, G.; Klein, D. R.; MacNeill, D.; Navarro-Moratalla, E.; Seyler, K. L.; Wilson, N.; McGuire, M. A.; Cobden, D. H.; Xiao, D.; Yao, W.; Jarillo-Herrero, P.; Xu, X. Electrical control of 2D magnetism in bilayer CrI3. *Nat. Nanotechnol.* **2018**, *13*, 544−548.

(23) Li, J.; Li, Y.; Du, S.; Wang, Z.; Gu, B.-L.; Zhang, S.-C.; He, K.; Duan, W.; Xu, Y. Intrinsic magnetic topological insulators in van der Waals layered MnBi2Te4-family materials. *Sci. Adv.* **2019**, *5*, eaaw5685.

(24) Fei, Z.; Huang, B.; Malinowski, P.; Wang, W.; Song, T.; Sanchez, J.; Yao, W.; Xiao, D.; Zhu, X.; May, A.; Wu, W.; Cobden, D.; Chu, J.-H.; Xu, X. Two-dimensional itinerant ferromagnetism in atomically thin Fe3GeTe2. *Nat. Mater.* **2018**, *17*, 778−782.

(25) Deng, Y.; Yu, Y.; Song, Y.; Zhang, J.; Wang, N.; Sun, Z.; Yi, Y.; Wu, Y.; Wu, S.; Zhu, J.; Wang, J.; Chen, X.; Zhang, Y. Gate-tunable room-temperature ferromagnetism in two-dimensional Fe3GeTe2. *Nature* **2018**, *563*, 94−99.

(26) Zhuang, H. L.; Kent, P. R. C.; Hennig, R. G. Strong anisotropy and magnetostriction in the two-dimensional Stoner ferromagnet Fe₃GeTe₂. *Phys. Rev. B: Condens. Matter Mater. Phys.* **2016**, *93*, 134407.

(27) Sarikurt, S.; Kadioglu, Y.; Ersan, F.; Vatansever, E.; Aktürk, O. Ü.; Yüksel, Y.; Akıncı, Ü.; Aktürk, E. Electronic and magnetic properties of monolayer α-RuCl 3: a first-principles and Monte Carlo study. *Phys. Chem. Chem. Phys.* **2018**, *20*, 997−1004.

(28) Ersan, F.; Vatansever, E.; Sarikurt, S.; Yüksel, Y.; Kadioglu, Y.; Ozaydin, H. D.; Aktürk, O. Ü.; Akıncı, Ü.; Aktürk, E. Exploring the electronic and magnetic properties of new metal halides from bulk to two-dimensional monolayer: RuX3 (X= Br, I). *J. Magn. Magn. Mater.* **2019**, *476*, 111−119.

(29) O'Hara, D. J.; Zhu, T.; Trout, A. H.; Ahmed, A. S.; Luo, Y. K.; Lee, C. H.; Brenner, M. R.; Rajan, S.; Gupta, J. A.; McComb, D. W.; et al. Room temperature intrinsic ferromagnetism in epitaxial manganese selenide films in the monolayer limit. *Nano Lett.* **2018**, *18*, 3125−3131.

(30) Tong, Y.; Guo, Y.; Mu, K.; Shan, H.; Dai, J.; Liu, Y.; Sun, Z.; Zhao, A.; Zeng, X. C.; Wu, C.; Xie, Y. Half-Metallic Behavior in 2D Transition Metal Dichalcogenides Nanosheets by Dual-Native-Defects Engineering. *Adv. Mater.* **2017**, *29*, 1703123.

(31) González-Herrero, H.; Gómez-Rodríguez, J. M.; Mallet, P.; Moaied, M.; Palacios, J. J.; Salgado, C.; Ugeda, M. M.; Veuillen, J.-Y.; Yndurain, F.; Brihuega, I. Atomic-scale control of graphene magnetism by using hydrogen atoms. *Science* **2016**, *352*, 437−441.

(32) Ma, Y.; Dai, Y.; Guo, M.; Niu, C.; Zhu, Y.; Huang, B. Evidence of the existence of magnetism in pristine VX2 monolayers (X= S, Se) and their strain-induced tunable magnetic properties. *ACS Nano* **2012**, *6*, 1695−1701.

(33) Zhou, Y.; Wang, Z.; Yang, P.; Zu, X.; Yang, L.; Sun, X.; Gao, F. Tensile strain switched ferromagnetism in layered NbS2 and NbSe2. *ACS Nano* **2012**, *6*, 9727−9736.

(34) Yun, W. S.; Lee, J. Strain-induced magnetism in single-layer MoS2: origin and manipulation. *J. Phys. Chem. C* **2015**, *119*, 2822−2827.

(35) Fert, A. Nobel lecture: Origin, development, and future of spintronics. *Rev. Mod. Phys.* **2008**, *80*, 1517.

(36) Oroszlány, L.; Deák, A.; Simon, E.; Khmelevskyi, S.; Szunyogh, L. Magnetism of gadolinium: a first-principles perspective. *Phys. Rev. Lett.* **2015**, *115*, 096402.

(37) Roth, D.; Bruckner, B.; Moro, M. V.; Gruber, S.; Goebl, D.; Juaristi, J. I.; Alducin, M.; Steinberger, R.; Duchoslav, J.; Primetzhofer, D.; Bauer, P. Electronic stopping of slow protons in transition and rare earth metals: breakdown of the free electron gas concept. *Phys. Rev. Lett.* **2017**, *118*, 103401.

(38) Tereshina, E.; Khmelevskyi, S.; Politova, G.; Kaminskaya, T.; Drulis, H.; Tereshina, I. Magnetic ordering temperature of nano-crystalline Gd: enhancement of magnetic interactions via hydro-genation-induced "negative" pressure. *Sci. Rep.* **2016**, *6*, 22553.

(39) Mendive-Tapia, E.; Staunton, J. B. Theory of Magnetic Ordering in the Heavy Rare Earths: Ab Initio Electronic Origin of Pair- and Four- Spin Interactions. *Phys. Rev. Lett.* **2017**, *118*, 197202.

(40) Nigh, H. E.; Legvold, S.; Spedding, F. H. Magnetism and Electrical Resistivity of Gadolinium Single Crystals. *Phys. Rev.* **1963**, *132*, 1092−1097.

(41) Cannon, J. F.; Cannon, D. M.; Tracy Hall, H. High pressure syntheses of SmB2 and GdB12. *J. Less-Common Met.* **1977**, *56*, 83−90.

(42) John, D.; Nharangatt, B.; Chatanathodi, R. Stabilizing honeycomb borophene by metal decoration: a computational study. *J. Mater. Chem. C* **2019**, *7*, 11493−11499.

(43) Li, W.; Kong, L.; Chen, C.; Gou, J.; Sheng, S.; Zhang, W.; Li, H.; Chen, L.; Cheng, P.; Wu, K. Experimental realization of honeycomb borophene. *Sci. Bull.* **2018**, *63*, 282−286.

(44) Dudarev, S. L.; Botton, G. A.; Savrasov, S. Y.; Humphreys, C. J.; Sutton, A. P. Electron-energy-loss spectra and the structural stability of nickel oxide: An LSDA+U study. *Phys. Rev. B: Condens. Matter Mater. Phys.* **1998**, *57*, 1505−1509.

(45) Zazoua, F.; Kacimi, S.; Djermouni, M.; Zaoui, A. Ab initio full-potential study of mechanical properties and magnetic phase stability of rare earth diboride compounds. *J. Appl. Phys.* **2011**, *110*, 014908.

(46) Hu, J.; Wang, P.; Zhao, J.; Wu, R. Engineering magnetic anisotropy in two-dimensional magnetic materials. *Adv. Phys-X* **2018**, *3*, 1432415.

(47) Vatansever, E.; Sarikurt, S.; Ersan, F.; Kadioglu, Y.; Üzengi Aktürk, O.; Yüksel, Y.; Ataca, C.; Aktürk, E.; Akıncı, Ü. Strain effects on electronic and magnetic properties of the monolayer α-RuCl 3: A first-principles and Monte Carlo study. *J. Appl. Phys.* **2019**, *125*, 083903.

(48) Gencer, H.; Izgi, T.; Kolat, V. S.; Atalay, S. Magnetic and magnetocaloric properties of GdB2 compound. *Optoelectron. Adv. Mater.* **2012**, *6*, 875−878.

(49) Ghader, D.; Khater, A. A new class of nonreciprocal spin waves on the edges of 2D antiferromagnetic honeycomb nanoribbons. *Sci. Rep.* **2019**, *9*, 1−12.

(50) Li, Z.; Cao, T.; Louie, S. G. Two-dimensional ferromagnetism in few-layer van der Waals crystals: renormalized spin-wave theory and calculations. *J. Magn. Magn. Mater.* **2018**, *463*, 28−35.

(51) An, Y.; Gong, S.; Hou, Y.; Li, J.; Wu, R.; Jiao, Z.; Wang, T.; Jiao, J. MoB2: a new multifunctional transition metal diboride monolayer. *J. Phys.: Condens. Matter* **2020**, *32*, 055503.

(52) Zhang, L.; Wang, Z.; Du, S.; Gao, H.-J.; Liu, F. Prediction of a Dirac state in monolayer TiB 2. *Phys. Rev. B: Condens. Matter Mater. Phys.* **2014**, *90*, 161402.

(53) Zhang, H.; Li, Y.; Hou, J.; Du, A.; Chen, Z. Dirac state in the FeB2 monolayer with graphene-like boron sheet. *Nano Lett.* **2016**, *16*, 6124−6129.

(54) Zhu, Z.; Tománek, D. Semiconducting layered blue phosphorus: a computational study. *Phys. Rev. Lett.* **2014**, *112*, 176802.

(55) Ersan, F.; Kecik, D.; Özçelik, V.; Kadioglu, Y.; Aktürk, O. Ü.; Durgun, E.; Aktürk, E.; Ciraci, S. Two-dimensional pnictogens: A review of recent progresses and future research directions. *Appl. Phys. Rev.* **2019**, *6*, 021308.

(56) Tokmachev, A. M.; Averyanov, D. V.; Parfenov, O. E.; Taldenkov, A. N.; Karateev, I. A.; Sokolov, I. S.; Kondratev, O. A.; Storchak, V. G. Emerging two-dimensional ferromagnetism in silicene materials. *Nat. Commun.* **2018**, *9*, 1−9.

(57) Tokmachev, A. M.; Averyanov, D. V.; Taldenkov, A. N.; Parfenov, O. E.; Karateev, I. A.; Sokolov, I. S.; Storchak, V. G. Lanthanide f 7 metalloxenes—a class of intrinsic 2D ferromagnets. *Mater. Horiz.* **2019**, *6*, 1488−1496.

(58) Sokolov, I.; Averyanov, D.; Parfenov, O.; Karateev, I.; Taldenkov, A.; Tokmachev, A.; Storchak, V. 2D ferromagnetism in europium/graphene bilayer. *Mater. Horiz.* **2020**, *7*, 1372.

(59) Zunger, A. Inverse design in search of materials with target functionalities. *Nat. Rev. Chem.* **2018**, *2*, 0121.